Improved performance of amorphous silicon solar cells via scattering from surface plasmon polaritons in nearby metallic nanoparticles

D. Derkacs, S. H. Lim, P. Matheu, W. Mar,[a] and E. T. Yu[b]
Department of Electrical and Computer Engineering, University of California, San Diego, La Jolla, California 92093-0407

(Received 17 February 2006; accepted 8 July 2006; published online 28 August 2006)

An engineered enhancement in short-circuit current density and energy conversion efficiency in amorphous silicon *p-i-n* solar cells is achieved via improved transmission of electromagnetic radiation arising from forward scattering by surface plasmon polariton modes in Au nanoparticles deposited above the amorphous silicon film. For a Au nanoparticle density of $\sim 3.7\times 10^8$ cm^{-2}, an 8.1% increase in short-circuit current density and an 8.3% increase in energy conversion efficiency are observed. Finite-element electromagnetic simulations confirm the expected increase in transmission of electromagnetic radiation at visible wavelengths, and suggest that substantially larger improvements should be attainable for higher nanoparticle densities. © *2006 American Institute of Physics*. [DOI: 10.1063/1.2336629]

Hydrogenated amorphous silicon (*a*-Si:H) solar cells have been of long-standing interest as a thin-film, low-cost alternative to bulk crystalline Si cells. Compared to crystalline Si, *a*-Si:H offers a much larger absorption coefficient across the solar radiation spectrum, as selection rules that apply to optical transitions in periodic crystals are relaxed in amorphous materials.[1] Thus, an *a*-Si:H film of thickness of ~500 nm absorbs sufficient sunlight to enable efficient solar cell operation, compared to thicknesses of several tens to hundreds of microns that are required for bulk crystalline Si devices.[2] However, the high defect densities typically present in *a*-Si:H thin films limit the typical minority carrier diffusion lengths to ~100 nm;[3] consequently, *a*-Si:H solar cells are generally fabricated using even thinner *a*-Si:H layers, resulting in reduced absorption of incident solar radiation.

A variety of approaches for increasing optical absorption in semiconductor materials based on excitation of surface plasmon polariton resonances in proximate metallic nanoparticles has been explored, frequently in the context of photovoltaic applications, for both organic[4–6] and solid-state device structures.[7–10] Most recently, studies have shown that spherical Au nanoparticles with diameters of 50–100 nm deposited on crystalline Si *p-n* junction photodiodes increase the absorption of light over a broad spectral range via the interaction of the incident electromagnetic radiation with surface plasmon polariton modes in the nanoparticles.[10] Because electromagnetic fields present in a semiconductor give rise to an optical transition rate proportional to the square of the electric field amplitude, the resulting increase in amplitude of the transmitted electromagnetic fields results in increased photogeneration of electron-hole pairs, and consequently increased photocurrent current in a *p-n* junction diode.

In this work, we have applied this concept to *a*-Si:H solar cells to achieve engineered enhancements in optical absorption, short-circuit current density, and energy conversion efficiency. At relatively modest nanoparticle densities, we obtain increases in short-circuit current density and energy conversion efficiency under halogen lamp illumination in excess of 8%, with finite-element electromagnetic simulations indicating that substantially larger increases should be possible at higher nanoparticle densities.

The basic device structure employed in these studies is shown in Fig. 1(a). 240 nm *a*-Si:H *p-i-n* structures were deposited by hot-wire chemical vapor deposition on stainless steel substrates. Contact patterns to the *p*-type surface were formed by optical lithography, followed by immersion in buffered oxide etch for 15 s to remove the surface oxide. A 20 nm indium tin oxide (ITO) contact layer was then deposited by rf sputtering for 3 min at 350 °C, and a standard lift-off procedure was then employed to produce circular diodes of 500 μm in diameter on a 5×5 mm^2 sample. Due to the short (~100 nm) minority carrier diffusion length of *a*-Si:H (Ref. 3) and the high sheet resistance of the *p*-layer, the active area of each diode was assumed to be equal to the

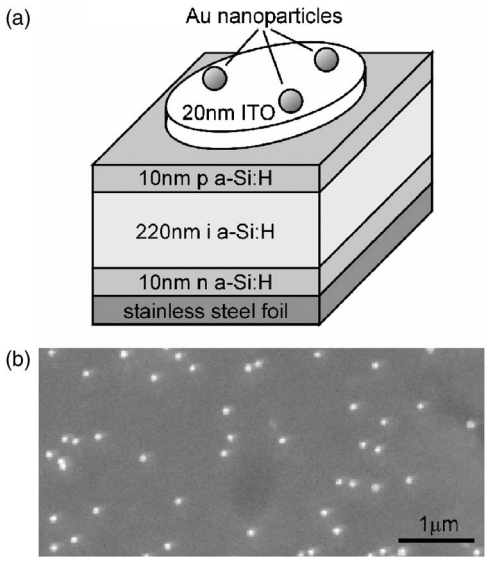

FIG. 1. (a) Schematic diagram of *a*-Si:H *p-i-n* solar cell structure with Au nanoparticle. (b) SEM image of 100-nm-diameter Au nanoparticles deposited on device surface at a concentration of 3.7×10^8 cm^{-2}.

[a]Present address: Department of Electrical Engineering, Stanford University, Stanford, CA 94305.
[b]Electronic mail: ety@ece.ucsd.edu

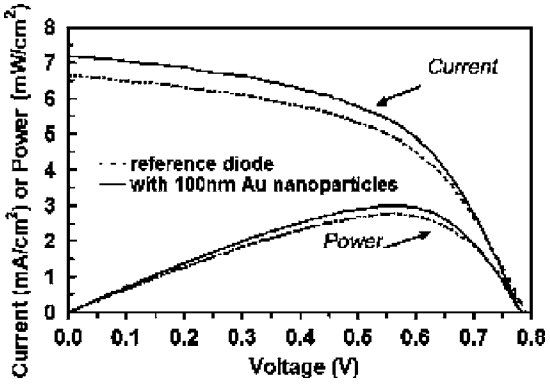

FIG. 2. *J-V* and power output curves for measured for reference diodes without Au nanoparticles (dashed lines), and for the same diodes after deposition of 100-nm-diameter Au nanoparticles (solid lines). Short-circuit current density and maximum power increase by 8.1% and 8.3%, respectively, for devices incorporating Au nanoparticles.

ITO contact area. This assumption does not affect the relative changes in short-circuit current density and energy conversion efficiency reported, although the absolute current density levels may be affected. Photovoltaic devices fabricated from the same *a*-Si:H samples using Pd metal contacts of ~15 nm in thickness yielded energy conversion efficiencies of approximately 5% under AM1.5 illumination.[11]

Following deposition of the ITO contacts, the device surface was subjected to a 5 min exposure to a poly-L-lysine solution and then a 4 min exposure to a solution containing 100 nm Au colloidal nanoparticles, and then blown dry with N_2. A 5 min oxygen cleaning was then used to remove residual poly-L-lysine from the surface, leading to more direct contact between the nanoparticles and the underlying ITO layer. To increase the concentration of nanoparticles on the surface, this deposition procedure was repeated up to five times; additional iterations typically resulted in clustering of nanoparticles on the surface. Scanning electron microscope (SEM) images, as shown in Fig. 1(b), confirmed that predominantly isolated Au nanoparticles were present, with a surface concentration of 3.7×10^8 cm^{-2}.

Current density versus voltage (*J-V*) characteristics were measured using a Hewlett-Packard 4150a semiconductor parameter analyzer. The diodes were illuminated using a fiber optic lamp with a 30 W quartz-halogen bulb, locked into position above the sample to provide illumination at normal incidence to the device surface. As references, *J-V* characteristics for each diode on each sample were measured both in the dark and under illumination prior to nanoparticle deposition. Following these initial measurements, Au nanoparticles were deposited, and *J-V* measurements were performed on eight devices both in the dark and under illumination. Standard deviations of only ~0.1 mA/cm^2 between diode *J-V* measurements were observed, and the *J-V* characteristics reported here represent averages across all diodes measured for each set of structures and measurement conditions.

J-V characteristics, and the corresponding power output, for the reference device structure without Au nanoparticles and for the same device structure following Au nanoparticle deposition are indicated by the dashed and solid lines, respectively, in Fig. 2. An 8.1% increase in short-circuit ($V=0$) current density, from 6.66 to 7.20 mA/cm^2, and an 8.3% increase in power output (and consequently in energy conversion efficiency), from 2.77 to 3.00 mW/cm^2, are observed for the device structure in which Au nanoparticles of concentration of 3.7×10^8 cm^{-2} have been incorporated. The different increases in short-circuit current density and energy conversion efficiency are a consequence of a slight increase in fill factor, from 52.6% to 52.8%, following nanoparticle deposition. We observed that the multiple cleanings performed as part of the nanoparticle deposition process can result in a rounding of the illuminated *J-V* curves, a decrease in short-circuit current density, typically by ~3%–5%, a substantial decrease in the open circuit voltage, and an increase in diode dark current, typically by a factor of 80–100. For example, a sample having a lower Au nanoparticle concentration of 1.75×10^8 cm^{-2} undergoing a more rigorous clean yielded a 7.5% increase in the short-circuit current density, from 6.85 to 7.35 mA/cm^2, but suffers from a decrease in the open circuit voltage, from 0.75 to 0.70 V, a decrease in the fill factor, from 49.0% to 48.5%, and a 1.2% decrease in the power output, from 2.52 to 2.49 mW/cm^2. Thus, the improvement in short-circuit current density and energy conversion efficiency arising specifically from the presence of the Au nanoparticles may in fact be larger than the increase determined from our measurements, but care in device processing must be exercised.

These results can be explained through a combination of the well-known Mie theory for isolated spherical particles, and—to account for the more elaborate geometry of the devices studied here—computational electromagnetic simulations. As light of wavelength λ interacts with small (diameter $d \ll \lambda$) metallic particles, extinction behavior due to resonant excitation of electron oscillations in the metal is observed as a distinct minimum in the transmission spectrum.[12] For particles with diameter below ~10 nm, only a single dipolar mode is supported; as the particle size increases, dipolar, quadrupolar, and other higher-order modes may be supported as well.

The total Mie extinction is a sum of contributions from absorption and from scattering associated with each supported surface plasmon polariton mode of the particle. For small particles supporting only dipolar modes, the total extinction cross section consists of a large absorption cross section and a smaller scattering cross section. For larger particles, with diameters of ~100 nm or larger, the opposite is true: although the total extinction cross section remains dominated by dipolar contributions, the scattering cross section is much larger than the absorption cross section. In addition, scattering from large particles at and above the Au nanoparticle resonant wavelength (~500 nm) is predominantly in the forward direction.[12]

The conclusion that visible light is forward scattered when incident on a single large nanoparticle is true in general for an ensemble of non-interacting particles suspended in a dielectric medium, and intuitively suggests that transmission of electromagnetic radiation into an appropriately positioned structure might be enhanced. However, for closely spaced particles on an absorbing substrate, particle-particle, particle-substrate, and particle-substrate-particle electromagnetic interactions complicate the propagation of the scattered field into the substrate. We have therefore performed finite-element electromagnetic simulations using FEMLAB™ for the geometry shown in Fig. 3. Simulations were performed for device structures with and without 100 nm Au nanoparticles on top of a 20 nm ITO contact and a 240 nm *a*-Si:H substrate; the dielectric functions for *a*-Si:H and ITO were ob-

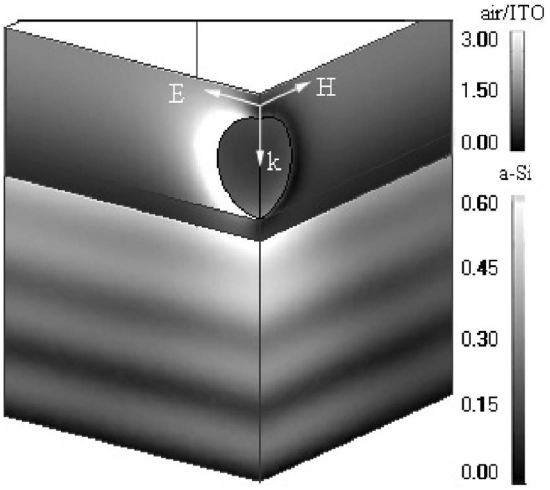

FIG. 3. Electromagnetic field amplitude distribution for a transverse electromagnetic wave at 600 nm wavelength incident on a structure consisting of a 100-nm-diameter Au sphere atop 20 nm ITO and 240 nm *a*-Si:H. Regions of high field amplitude are evident to the left of the particle (arising from the particle surface plasmon polariton resonance) and below the particle (arising from forward scattering of the incident wave).

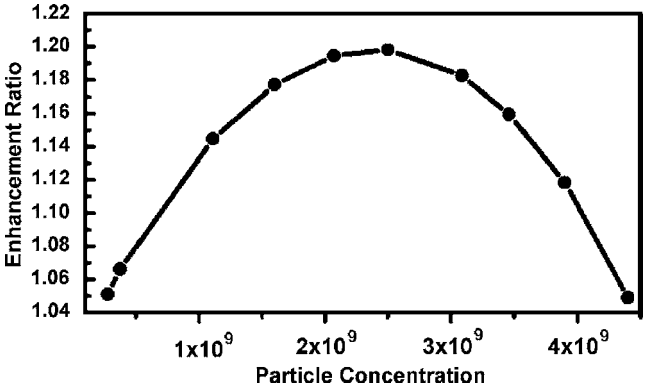

FIG. 4. Ratio R_p of $|E_0|^2$, integrated over the *a*-Si:H layer, for devices incorporating Au nanoparticles to that for reference devices without Au nanoparticles, as a function of particle density, computed for incident electromagnetic radiation at $\lambda=600$ nm.

tained from Refs. 13 and 14, respectively. A reflective boundary condition was applied beneath the *a*-Si:H layer to model the stainless steel substrate. Quarter-plane symmetry was used for computational efficiency, and periodic boundary conditions were employed resulting in simulation of a periodic array of nanoparticles atop the ITO/*a*-Si:H thin-film structure. Transverse electromagnetic waves were launched from above the substrate and nanoparticle, if present, with wave vector normal to the substrate surface.

Figure 3 shows the amplitude of the simulated electric field for an incident wave with $\lambda=600$ nm and effective particle density of 3.7×10^8 cm^{-2}. The dipole-like surface plasmon polariton resonance of the nanoparticle results in the enhanced electric field amplitude to the left of the nanoparticle, and as postulated we observe an enhanced electric field amplitude in the *a*-Si:H layer below the nanoparticle, which arises due to forward scattering of the incident wave by the nanoparticle. The oscillations visible in the *a*-Si:H are a consequence of the reflecting boundary created by the stainless steel substrate.

To estimate the influence of this field on the optical transition rate in the *a*-Si:H layer, and consequently on the photogenerated current, we note that the optical transition rate is proportional to the square of the electric field amplitude, $|E_0|^2$. Thus, computation of the ratio R_p of $|E_0|^2$, integrated over the entire *a*-Si:H layer, for a structure with an Au nanoparticle present to that for a structure with no nanoparticle should provide a very approximate measure of the relative change in photogenerated current for light incident at a single wavelength due to the presence of the Au nanoparticle. Figure 4 shows this ratio, derived from our simulations for an incident electromagnetic wave with wavelength of 600 nm, as a function of Au nanoparticle density. While this relatively simple calculation does not provide a quantitative prediction of the corresponding increase in photogenerated current, it is clear that a substantially larger increase than that observed in our experiments should be attainable at higher particle densities. At a wavelength of 600 nm, a particle density of $\sim2.5\times10^9$ cm^{-2} appears to be optimal, resulting in an increase in R_p approximately three times larger than that at the concentration present in our experiments.

In summary, we have fabricated and characterized *a*-Si:H thin-film solar cells in which Au nanoparticles have been employed to engineer the transmission and spatial distribution of electromagnetic fields within the *a*-Si:H layer, resulting in an increase of 8.1% in short-circuit current density and 8.3% in energy conversion efficiency compared to values achieved in reference devices without Au nanoparticles. Computational electromagnetic simulations confirm that the presence of the Au nanoparticles results in increased transmission into and concentration of electromagnetic fields within the *a*-Si:H layer, and indicate that substantially larger increases should be possible at higher particle densities.

Part of this work was supported by a grant from the UCSD Von Liebig Center and through the University of California CLC program. The authors would like to acknowledge helpful discussions with C.-S. Jiang, and Y. Q. Xu from the U.S. National Renewable Energy Laboratory for providing *a*-Si:H thin films for this work.

[1] A. Luque and S. Hegedus, *Handbook of Photovoltaic Science and Engineering* (Wiley, Chichester, 2003), Chap. 12, pp. 514-518.
[2] A. Goetzberger, C. Hebling, and H.-W. Schrock, Mater. Sci. Eng., R. **R40**, 1 (2003).
[3] A. V. Shah, H. Schade, M. Vanecek, J. Meier, E. Fallat-Sauvain, N. Wyrsch, U. Kroll, C. Droz, and J. Bailat, Prog. Photovoltaics **12**, 113 (2004).
[4] M. Westphalen, U. Kreibig, J. Rostalski, H. Lüth, and D. Meissner, Sol. Energy Mater. Sol. Cells **61**, 97 (2000).
[5] O. Stenzel, S. Wilbrandt, A. Stendal, U. Beckers, K. Voigtsberger, and C. von Borczyskowski, J. Phys. D **28**, 2154 (1995).
[6] O. Stenzel, A. Stendal, K. Voigtsberger, and C. von Borczyskowski, Sol. Energy Mater. Sol. Cells **37**, 337 (1995).
[7] H. R. Stuart and D. G. Hall, Appl. Phys. Lett. **69**, 2327 (1996).
[8] H. R. Stuart and D. G. Hall, Appl. Phys. Lett. **73**, 3815 (1998).
[9] H. R. Stuart and D. G. Hall, Phys. Rev. Lett. **80**, 5663 (1998).
[10] D. M. Schaadt, B. Feng, and E. T. Yu, Appl. Phys. Lett. **86**, 063106 (2005).
[11] C.-S. Jiang (private communication).
[12] C. F. Bohren and D. R. Huffman, *Absorption and Scattering of Light by Small Particles* (Wiley, New York, 1983), p. 329.
[13] E. D. Palik, *Handbook of Optical Constants of Solids* (Academic, San Diego, CA, 1985), 1, pp. 290-291.
[14] D. Mergel and Z. Qiao, J. Phys. D **35**, 794 (2002).